Journal of Power Sources 196 (2011) 5453–5469

Contents lists available at ScienceDirect

Journal of Power Sources

journal homepage: www.elsevier.com/locate/jpowsour

Controlling gas diffusion layer oxidation by homogeneous hydrophobic coating for polymer electrolyte fuel cells

Yusuke Hiramitsu*, Hitoshi Sato, Kenji Kobayashi, Michio Hori

Fuel Cell Research Center, Daido University, 10-3 Takiharu-cho, Minami-ku, Nagoya 457-8530, Japan

ARTICLE INFO

Article history:
Received 21 June 2010
Received in revised form 10 January 2011
Accepted 31 January 2011
Available online 17 February 2011

Keywords:
Polymer electrolyte fuel cell (PEFC)
Water management
Water flooding
Gas diffusion layer (GDL)
Durability
Long-term performance

ABSTRACT

Reduced production costs and enhanced durability are necessary for practical application of polymer electrolyte fuel cells. There has been a great deal of concern about degradation of the gas diffusion layer located outside the membrane electrode assembly. However, very few studies have been carried out on the degradation process, and no suitable methods for improving the durability of the cell have been found.

In this work, the influence on the cell performance and factors involved in the degradation of the gas diffusion layer has been clarified through power generation tests.

Long-term power generation tests on single cells for 6000 h were carried out under high humidity conditions with homogeneous and inhomogeneous hydrophobic coating gas diffusion layers. The results showed that the increase in the diffusion overvoltage from the gas diffusion layer could be controlled by the use of a homogeneous coating. Post-analyses indicated that this occurred by controlling oxidation of the carbon fiber.

1. Introduction

The durability of the various elements in polymer electrolyte fuel cells (PEFCs) must be improved in order to allow practical applications of these cells to become possible. To achieve this, it is important to independently assess the degradation mechanisms of each element to qualitatively determine correlations between them [1,2].

A PEFC consists of a central proton conductive membrane sandwiched by a catalyst layer (CL) and a gas diffusion layer (GDL) on each side; this combined structure is referred to as a membrane electrode assembly (MEA) and has a carbon or metallic separator on each side. Generically, the CL is formed from a Pt-catalyst on a high specific surface area carbon support and a polymer electrolyte similar to a membrane. Carbon black is normally used for the carbon support since it exhibits high electron conductivity, high specific surface area and forms a corrosion-resistant electrode. Carbon paper is generally used for the GDL, in which high electron conductivity, high gas diffusivity and corrosion resistance are demanded.

PEFCs are generally operated under high humidity conditions created by an external humidifier in addition to the presence of electrochemically produced water at the cathode; this is because sulfo-group proton conducting polymers exhibit optimal performance under such conditions. On the other hand, during high-load operation, water condensation can occur at the electrode, and the gas diffusion overvoltage increases due to inhibition of gas diffusion. This phenomenon is referred to as flooding, and it gives rise to instability and power reduction. Therefore, optimization of the waterproofing treatment and the structure of the CL or GDL to prevent such flooding are important [3–6], and this is referred to as water management.

Even if such water management methods are applied to the GDL, increasing gas diffusion overvoltage still occurs during long-term operation as a result of degradation of both the CL and GDL [7–9].

Many studies have focused on the corrosion of the catalyst carbon support. It was reported to be accelerated by the start/stop cycle with an anode air purge or the load change cycle for focusing the vehicle [10–14]. Furthermore, the details of the degradation mechanism have also been clarified by testing of model carbonaceous materials such as graphite [15–19]. Research into the use of carbon substitution materials such as conductive oxidation products in order to suppress corrosion is also ongoing [20–22].

In addition, the CL allows gas diffusion due to its porous structure, and it has been shown that, during long-term operation, a

* Corresponding author. Tel.: +81 52 612 6144; fax: +81 52 612 6144.
E-mail addresses: hiramitu@daido-it.ac.jp (Y. Hiramitsu), h-sato@daido-it.ac.jp (H. Sato), k3kenji@daido-it.ac.jp (K. Kobayashi), hori@daido-it.ac.jp (M. Hori).

0378-7753/$ – see front matter © 2011 Elsevier B.V. All rights reserved.
doi:10.1016/j.jpowsour.2011.01.099

loss of diffusivity occurs due to a decrease in the pore volume in the absence of corrosion [7–9].

On the other hand, there have been very few studies addressing the reduction of the hydrophobicity of the GDL. It has been reported that this occurs due to oxidation of the GDL and degradation of the PTFE [23–30]. However, the effects of GDL degradation on the cell performance have not yet been established, nor has a clear mechanism been presented.

It is estimated that degradation of gas diffusivity is different by the manufacturing method and a waterproofing treatment of GDL. In the long-term operating test of the PEFC, there are little results that gas diffusivity degradations of CL and/or GDL were separated. This is because the separating observation of the gas diffusivity decrease due to CL and/or GDL is difficult. However, CL and GDL are components which pass through a different manufacture process. If those degradations are separated, it is useful for developers.

Therefore, it is necessary to clarify the relation between GDL degradation and GDL properties, and to improve the cell lifetime and durability by identifying the long-term degradation mechanism of the GDL.

The purpose of the present study is to obtain fundamental information concerning the decrease in the hydrophobicity of the GDL in PEFCs under normal operating conditions. Changes in the polarization during long-term operation were examined using GDLs with two different types of waterproofing treatment. The gas diffusivity decrease of GDL was specified using GDL used for these long-term operations and unused GDL.

In addition, post-analyses of GDL were carried out to clarify the mechanism behind the observed decrease in hydrophobicity.

This study adopted waterproofing method of GDL as the experimental parameter to clarify the degradation mechanism of GDL. Meanwhile, the water management property of GDL affects the moisture state at CL simultaneously. The corrosion of carbon support in CL is different with its moisture states [9]. Moreover, water management GDL may control flooding at CL/GDL interface [5,6] due to CL degradation. Therefore, not only GDL degradation evaluation but CL degradation evaluation was performed.

2. Experimental

2.1. Long-term operation test

2.1.1. GDL and waterproofing treatment

Carbon paper with a thickness of 110 μm (TGP-H-H030, Toray Industries, Inc., Japan) was used for the GDL. Two different waterproofing methods were used.

The first was treatment with hydrophobic particles by submerging the GDL in a 12-wt% PTFE dispersion (31-JR, DuPont-Mitsui Fluorochemicals Co. Ltd., Japan), followed by drying and heat treatment for 15 min at 350 °C. The mean PTFE particle diameter was 0.2–0.25 μm. An atomic force microscopy (AFM) image of the treated surface of the carbon fiber is shown in Fig. 1, where regions of PTFE adhesion can be seen alternating with exposed regions of the carbon surface.

The second treatment involved the formation of a hydrophobic coating by submerging the GDL in a 1-wt% polyperfluoro[4-vinyloxy-1-butene] solution (Diluted Cytop CTL-109AE by CT-Solv.100E, Asahi Glass Co. Ltd., Japan), followed by drying and heat treatment for 15 min at 60 °C. The chemical structure of Cytop is shown in Fig. 2. It is a fusible material and can form a homogeneous hydrophobic coating on carbon fiber.

In this report, the former type of waterproofed GDL is referred to as an inhomogeneous coating GDL and the latter as a homogeneous coating GDL. Each GDL was assembled in MEA without the microporous layer.

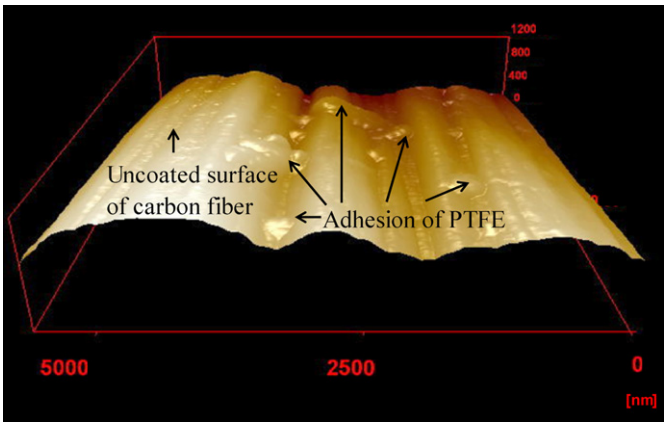

Fig. 1. AFM observation of carbon fiber with PTFE treatment.

2.1.2. Membrane electrode assembly

The MEA consisted of a commercially available catalyst-coated membrane (CCM) which was sandwiched between the waterproofed GDLs described in Section 2.1.1. Pt particles supported by carbon black were used for the catalyst. The Pt loading was 0.3 mg cm^{-2} in both the anode and cathode, and the electrode area was 3 cm × 15 cm. A 30-μm-thick perfluorosulfonic acid membrane was used as a proton exchange membrane (PEM). A perfluorosulfonic acid ionomer was used as an ionomer in CL.

2.1.3. Structure of single cell

Fig. 3 shows the structure of the single cells constructed for this investigation. Each cell consisted of a CCM at the center with a GDL and carbon separator on each side. Sixteen straight 1-mm wide channels were machined into the separator, with lengths of 150 mm and spacings of 1 mm. The channel structure is shown in Fig. 4. The depths of the channels were 0.5 mm at the cathode and 0.4 mm at the anode. The fuel and oxidant were carried away in a counter-flow configuration.

2.1.4. Long-term operation tests

The long-term operation tests were conducted at constant current of 0.3 A cm^{-2}, cell temperature of 75 °C, humidifier temperature of 70 °C, with pure H_2 utilization of 70% at the anode (0.135 L min^{-1}), and air utilization of 40% at the cathode (0.56 L min^{-1}) under atmospheric pressure. The cell resistance was measured using a milliohm meter at high-frequency. The humidifier was a bubbler containing pure water.

2.2. Fuel cell diagnoses

The polarization curves were regularly observed during the durability test for long-term power generation. After observations

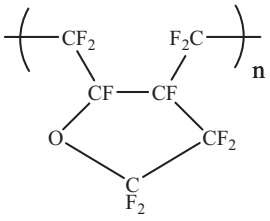

Fig. 2. The chemical structure of Cytop (polyperfluoro[4-vinyloxy-1-butene]) for homogeneous coating.

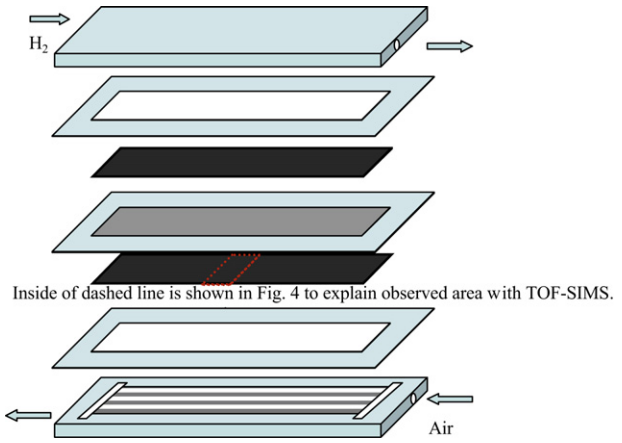

Fig. 3. Detailed view of a single cell prepared for the long-term operation test.

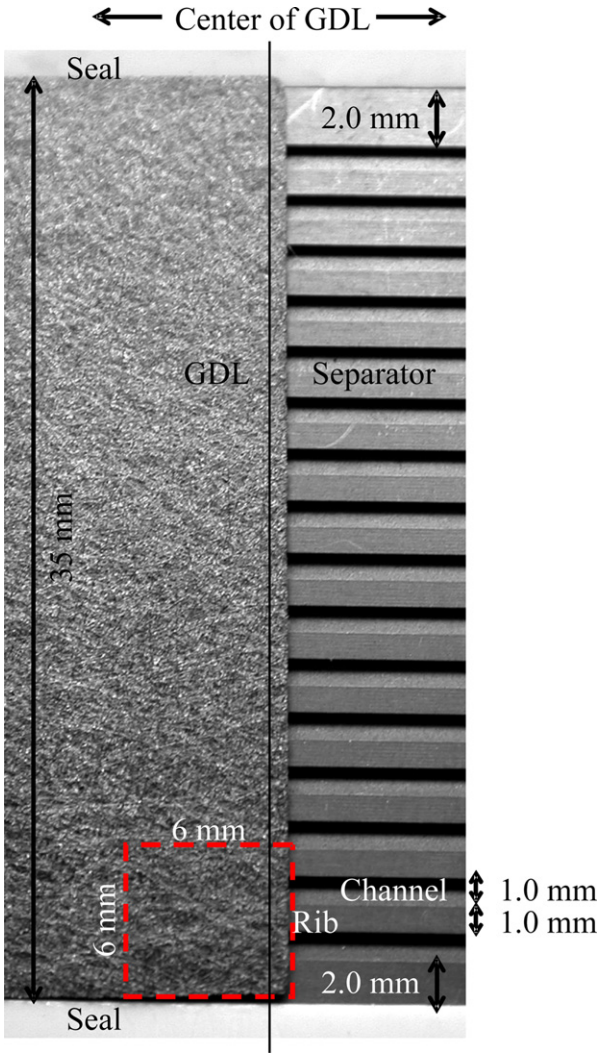

Fig. 4. Detailed view of observation area of GDL with TOF-SIMS.

were completed, operation was stopped, the cathode gas supply was changed from air to N_2, and the electrochemical properties of the cell were inspected. After these measurements were completed, the long-term test was re-started. Cell diagnosis was periodically conducted using such a sequence.

2.2.1. Polarization curves

The polarization curves were regularly measured during long-term operation under the same generating conditions [7–9]. The pretreatment of the polarization measurement was as follows. Cell voltage was held 10 s or more at the open-circuit voltage (OCV), current density was increased until cell voltage became about 0.2 V, and it was decreased to zero. After pretreatment, the OCV was held for 10 s, current density was increased until cell voltage became about 0.2–0.1 V, and the polarization curve was obtained. The load current was increased and decreased at a rate of 5 A min^{-1} with constant gas utilization same as long-term operation. The flow rate of H_2 and air at OCV were set to 0.04 and 0.12 L min^{-1}, respectively.

In the polarization curve, the cell voltage is decreased with respect to OCV E_{OCV} by the following factors (see Eq. (1)): the resistance overpotential $\eta_{Resistance}$ (see Eq. (2)), the activation overpotential $\eta_{Activation}$ (see Eq. (3)), and the diffusion overpotential $\eta_{Diffusion}$ (see Eq. (4)).

The polarization analysis was performed to fit the experimental polarization curves by Eq. (1) using the least-squares method as demonstrated in Fig. 6.

$$E(i) = E_{OCV} - \eta_{Resistance}(i) - \eta_{Activation}(i) - \eta_{Diffusion}(i) \quad (1)$$

$$\eta_{Resistance}(i) = Ri \quad (2)$$

$$\eta_{Activation}(i) = b_1 \ln \frac{i + i_c}{i_0} \quad (3)$$

$$\eta_{Diffusion}(i) = b_2 \ln \frac{i_{lim}}{i_{lim} - (i + i_c)} \quad (4)$$

where E is the cell voltage, E_{OCV} the open circuit voltage, b_1 the Tafel slope at low current density, i the current density, i_0 the exchange current density, i_c the leak current density, b_2 the Tafel slope at high current density, i_{lim} the limiting current, R the cell resistance, and $\eta_{diffusion}$ is the diffusion overpotential. The theoretical E_{OCV} of 1.23 V was used. Here, $\eta_{Resistance}$ was calculated using the instantaneously measured high-frequency resistance R. i_c was assigned leak current density measured in Section 2.2.2. In the polarization curve analysis, the anode polarization was neglected.

2.2.2. Chronocoulometry

After measurement of the polarization curve, operation was stopped, the cathode gas was switched from air to N_2, and the electrochemical properties were then measured.

Chronocoulometry (CC) was used to assess the H_2 crossover rate as an indicator of degradation of the PEM; the measurements were carried out using a potentiostat [7–9]. The H_2 gas crossover rate from anode being supplied with H_2 to the cathode being supplied with N_2 is estimated as the H_2 oxidation current at cathode. The cell and humidifier temperatures were the same as those used during the long-term operation test. The H_2 was supplied at 0.09 L min^{-1} and the N_2 at 0.38 L min^{-1}. After these measurements were completed, the long-term test was re-started. Cell diagnosis was periodically conducted using such a sequence.

2.3. Identification of degraded components

Degraded components were identified to determine which component contributed more to the overall degradation of the fuel cell [7–9].

The CCM and GDL were replaced after completion of the 6000 h operation test. The spent components were replaced with a newly aged CCM and GDL, and the rebuilt fuel cell was operated for further diagnosis. The components were combined as shown in Table 1 to create the rebuilt MEAs, and their polarization curves were measured.

Table 1
Combinations of MEA components for determining the GDL degradation level.

MEA no.	CCM condition	GDL water-proof treatment method	GDL condition
1	New	Homogeneous coating	New
2	New	Homogeneous coating	Operated for 6000 h
3	New	Inhomogeneous coating	New
4	New	Inhomogeneous coating	Operated for 6000 h

2.4. Post-analysis to evaluate CL and GDL degradation

2.4.1. CCM morphology and cross-section analysis with electron probe microanalysis

An elemental mapping of the cross-section of each CCM was obtained using an electron probe microanalyzer (EPMA, EPMA-1610, Shimadzu Corp., Japan) in order to evaluate degradation of each CCM. The thickness of the CL was also estimated from the backscattered electron images (BEIs) of the cross-section of each CCM.

2.4.2. Measurement of pore diameter distribution in the CL using mercury intrusion porosimetry

In order to evaluate changes in the porous structure of the CL on a CCM, the pore structure of the CL was measured using mercury intrusion porosimetry (MIP, Poresizer 9320 Micromeritics Instrument Corp., USA). In order to avoid destruction of the void structure, when stripping the CL from the membrane, the measurements were carried out with the CLs still on both the anode and the cathode, because small pores from the PEM applied to the CL were not detected by MIP. Therefore, the obtained pore structure was the mean of the structures on the anode and cathode. Also, the mean thickness of the CL was measured using the BEI. This pore parameters obtained by MIP were normalized to the volumetric by dividing thickness.

2.4.3. Evaluation of the catalyst carbon support crystallinity by laser Raman spectroscopy

Raman spectra were observed to estimate the structural changes of the carbon support in the CL [9,14] using laser Raman spectrometer (T-64000, Horiba, Ltd., Japan). Raman spectroscopy has been applied for many carbonaceous materials, from graphite to carbon black and activated carbon, and the spectral changes are well known to depend on the average size of the crystalline domains. The 514.5 nm laser line was used for the excitation with approximately 1 mW of power and a 100 μm laser spot at the sample.

2.4.4. Wettability measurement of GDL

In order to quantify the change in the wettability of the GDL, the dynamic contact angles of the GDL were measured according to the Wilhelmy method with DCAT21 (DataPhysics Instruments GmbH, Germany). Because the Wilhelmy method evaluates the contact angle using a boundary line, it is less sensitive to large variations in the hydrophobicity and structure of the GDL carbon paper than the sessile drop or water permeametry methods, and allows reproducible measurements. However, the wettabilities of both sides of the GDL are measured as one. The GDL was cut into a 10 mm × 35 mm strip specimen which was dipped vertically into pure water. In the Wilhelmy method, the contact angle θ, the measured weight m and the immersion depth h are related by Eq. (5). The contact angle θ is obtained from the intercept by extrapolating to an immersion depth $h = 0$ in order to cancel the buoyancy force.

$$mg = L\gamma_{water} \cos\theta - sh\rho_{water}g \quad (5)$$

where g is the gravitational acceleration, L the boundary length of GDL sample, γ_{water} the surface tension of water, s the cross-sectional area of GDL sample, and ρ_{water} is the density of water.

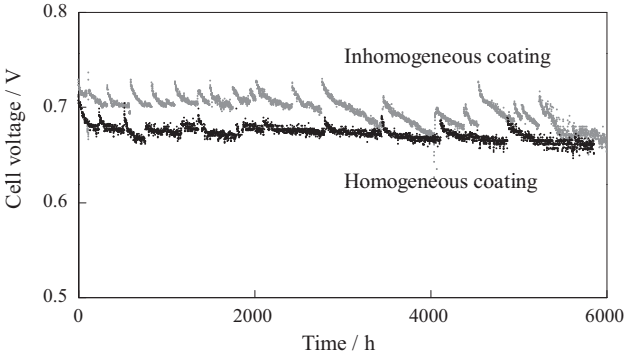

Fig. 5. Time-based voltage changes during long-term operation at a current density of 0.3 A cm^{-2} with inhomogeneous or homogeneous coating GDL.

2.4.5. Elemental analysis of the GDL with EPMA

The oxygen and fluorine content of each GDL were determined using EPMA in order to evaluate the degree of degradation. This technique can identify the elements in compounds on the carbon-fiber surface. Time change of the O intensity was calculated from the mapping area which was detected strong O signal especially, after removing the background and standardized by F intensity.

2.4.6. Identification of surface adsorbates on the GDL using time-of-flight secondary ion mass spectrometry

Time-of-flight secondary ion mass spectrometry (TOF-SIMS; TOF.SIMS 5, ION-TOF GmbH, Germany), which measures the masses of positive and negative ions ejected from the surface during bombardment with Bi_3^{2+} ions, was performed to identify the chemical species present in surface organic adsorbates in a 6 mm × 6 mm region of the GDL. In order to determine whether the degraded area of the GDL was facing the rib or the channel of the separator, the GDL sampling area was defined as shown in Fig. 4. Since TOF-SIMS is capable of identifying chemical compounds on the carbon-fiber surface, the results obtained complement the EPMA results. Furthermore, TOF-SIMS is more sensitive than EPMA, particularly to surfaces. Peak intensity was calculated from the 2 mm × 6 mm area corresponding to contact face of the channel and the rib of separator which are shown in Fig. 19(a).

3. Results

3.1. Long-term operation

3.1.1. Time-dependence of cell characteristics

The variations in cell voltage with time during long-term operation with a 0.3 A cm^{-2} load are shown in Fig. 5. A decrease in the cell voltage is observed for both GDLs.

These decreases were analyzed to decouple the polarization curves at higher current density of 0.6 A cm^{-2} in order to evaluate the changes in gas diffusivity.

The initial performance of MEA using GDL which applied each waterproofing treatment is shown in Fig. 6. Although the initial performance was almost comparable, homogeneous coating GDL showed smaller diffusion overvoltage.

Fig. 7 shows the time-based changes in $\eta_{Activation}$, $\eta_{Resistance}$ and $\eta_{Diffusion}$ at current density of 0.6 A cm^{-2}. $\eta_{Activation}$ and $\eta_{Resistance}$ remained almost constant. Although the activation overvoltage of the cell using homogeneous coating GDL was high, it originated in the variation of the CL performance on CCM. Because activation overpotential was smaller than this when only CCM was exchanged for a new one, as shown in Fig. 9. In contrast, $\eta_{Diffusion}$ exhibited a different behavior for each of the GDLs, significantly increasing

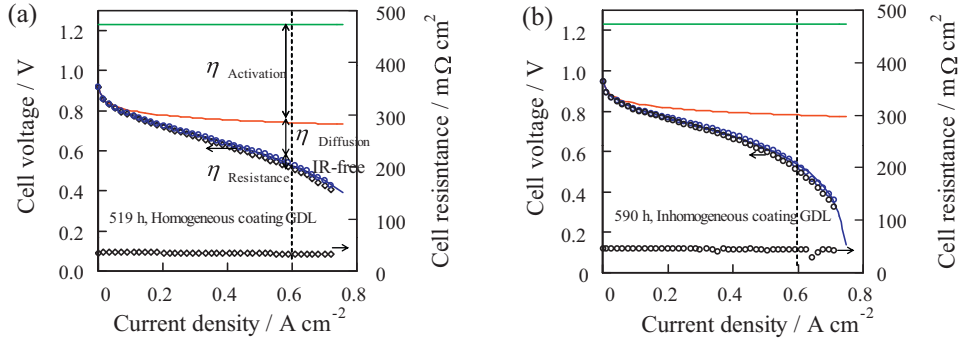

Fig. 6. Demonstration of the polarization analysis with experimental data of each GDL at the initial performance. (a) Polarization with homogeneous coating GDL; (b) polarization with inhomogeneous coating GDL.

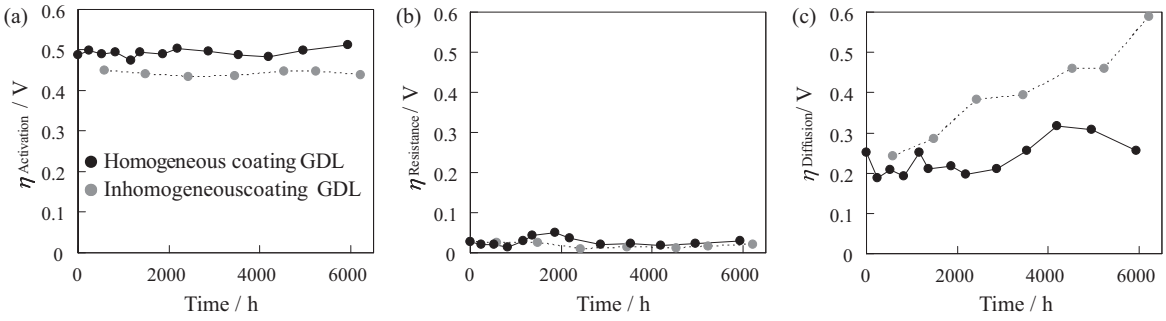

Fig. 7. (a) Activation overpotential $\eta_{Activation}$, (b) resistance overpotential $\eta_{Resistance}$, and (c) diffusion overpotential $\eta_{Diffusion}$ estimated from the polarization curve conducted during the long-term operation test at a current density of 0.6 A cm^{-2}.

with time for the inhomogeneous coating GDL but remaining in slight increase for the homogeneous coating GDL.

Fig. 8 shows the time-based changes in the leakage current density due to H_2 crossover calculated from the CC results. For both GDLs, the leakage current density remained almost unchanged over 6000 h of operation. The H_2 crossover rate increases with thinning and degradation of the membrane, but is appears that such degradation was negligible for both GDLs.

3.1.2. Identification of deteriorated components

Fig. 9 shows polarization curves for combinations of new or spent homogeneous coating GDL components. The specific combinations are listed in Table 1. The polarization curves for both MEAs are almost identical. The homogeneous coating GDL operated for 6000 h suffered little or no degradation during power generation at 81% RH. This indicates that there was almost no GDL degradation with increasing wettability.

Fig. 10 shows polarization curves for combinations of new or spent inhomogeneous coating GDL components. The active areas of these MEAs were only 30 mm × 25 mm because some parts of the GDL were sampled for post-analysis before these tests. The cell voltage at high current density at 81% RH is seen to decrease following 6000 h operation due to an increase in the diffusion overvoltage. This indicates GDL degradation with increasing wettability.

3.2. Post-analysis

3.2.1. Pt mapping of CCM cross-section with EPMA

Fig. 11 shows the distribution of Pt on the CCM cross-sections obtained with EPMA mapping. The layer with a high concentration of Pt was the CL, and the membrane was between two CLs. Comparison of the new CCM with the CCMs employed in long-term operating tests showed that the latter had a slight

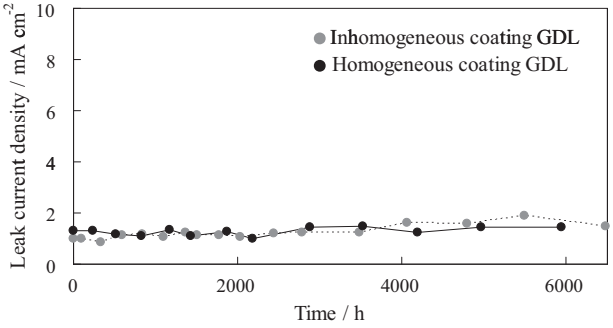

Fig. 8. Time-based changes in crossover H_2 flow rate, evaluated in terms of leak current density by CC.

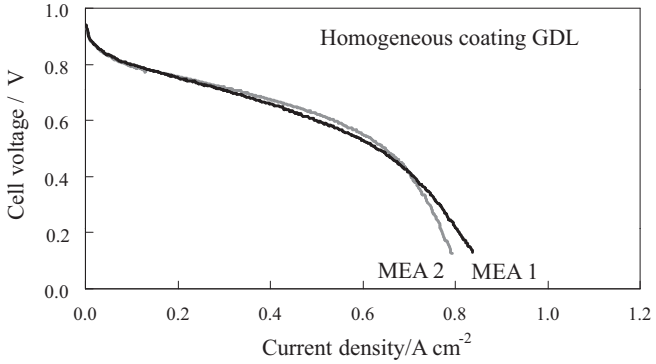

Fig. 9. Polarization curves of MEAs after exchange of homogeneous coating GDL, as indicated in Table 1. Active area of MEAs was 45 cm^2.

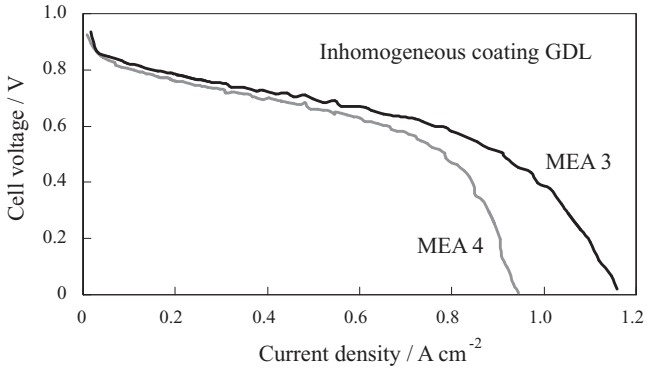

Fig. 10. Polarization curves of MEAs after exchange of inhomogeneous coating GDL, as indicated in Table 1. Active area of MEAs was 7.5 cm^2.

Table 2
CL pore parameters measured with MIP.

	Pore volume ($cm^3\ cm^{-3}$)	Peak pore diameter (nm)
100 h	0.44	57
Homo-coat 6000 h	0.42	56
Inhomo-coat 6000 h	0.33	58

increase of Pt signal in the CL. The thicknesses of the CL measured from the BEIs were 10.8 μm for the new anode and new cathode, 10.9 and 10.4 μm for the anode and cathode operated with homogeneous coating GDL, and 13.6 and 13.4 μm for the anode and cathode operated with inhomogeneous coating GDL, respectively.

3.2.2. Pore structure of the CL by MIP

Table 2 shows the CL pore volume cumulated pores from 10 to 1000 nm and peak pore diameter determined by MIP. The pore volume of the CL decreased more using inhomogeneous coating GDL than homogeneous coating GDL. Each change of the peak pore diameter is small.

3.2.3. Raman spectra of carbon support

Fig. 12 shows Raman spectrum parameters of carbon support calculated from spectra of the CL. For the comparison of the Raman spectra, full width at half maximum (FWHM, denoted as ΔG), the G band position and relative band intensity (I_D/I_G) were calculated.

Table 3
Contact angles of GDLs.

Homogenous coating GDL	Advancing contact angle	Receding contact angle
100 h operated	172°	108°
6000 h operated	167°	96°

Comparison of these parameters indicated that the operated CLs exhibited higher G band positions and smaller ΔG and smaller I_D/I_G. This change suggested oxidation of the carbon support. Furthermore, the tendency was greater for the CLs operated with homogeneous coating GDL.

3.2.4. Wettability measurements of GDL

Hysteresis curves of wettability of the homogeneous coating GDL determined using the Wilhelmy method are shown in Fig. 13. For advancing immersion, the curves for GDLs operated for 100 and 6000 h are almost identical. However, during receding immersion, it can be seen that the GDL operated for 6000 h exerted a stronger pull than the GDL operated for 100 h. Table 3 shows the contact angles of the homogeneous coating GDLs. The advancing and receding contact angles for the GDL operated for 100 h were extremely large, indicating high hydrophobicity. However, for the GDL operated at 6000 h, the advancing contact angle was 5–6° smaller and the receding contact angle was 11–12° smaller than for the 100 h case. As shown in Section 3.1.2, the cell performances with these GDLs were almost identical, although changes in the wettability of the GDL had occurred.

3.2.5. Elemental analysis on the GDL with EPMA

Fig. 14 shows EPMA O mappings of the GDLs. The homogeneous coating GDLs exhibited stronger oxygen signals due to the oxygen content of the Cytop coating (see Fig. 2). O mappings of the homogeneous coating GDLs following 6000 h operation are shown in Fig. 14 (Homo-a 6000 h), (Homo-b 6000 h) and (Homo-c 6000 h), for the surfaces (a), (b) and (c) indicated in the inset. There are no characteristic patterns in the oxygen distribution at any of these regions. For the cathode channel side of the inhomogeneous coating GDL following 6000 h operation, however, a clear oxygen pattern was found, as shown in Fig. 14 (Inhomo-a 6000 h), which reflected the channel pattern. There was no such pattern found on the CL side of the same GDL, as shown in Fig. 14 (Inhomo-b 6000 h). In addition, no pattern was observed on the channel side of the anode GDL, as seen in Fig. 14 (Inhomo-c 6000 h).

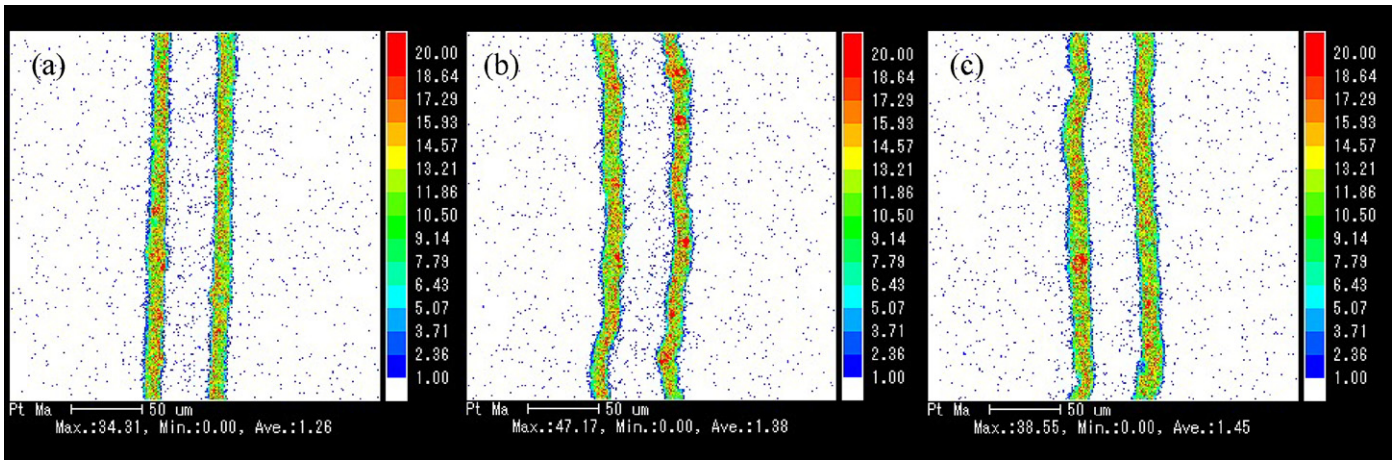

Fig. 11. Pt mapping of the CCM cross-section with EPMA. Left side is anode and right side is cathode. (a) CCM conditioned for 100 h. (b) CCM after 6000 h operation with homogeneous coating GDL. (c) CCM after 6000 h operation with inhomogeneous coating GDL.

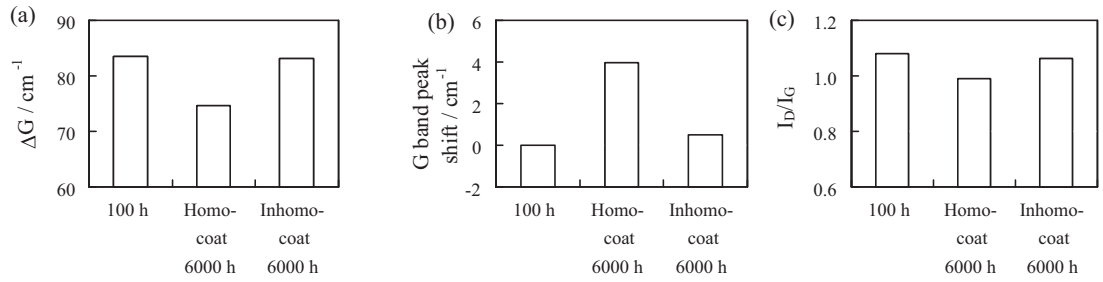

Fig. 12. (a) G band half-widths calculated from laser Raman spectra for the cathode carbon support, (b) G band shifts, and (c) I_D/I_G.

These were subject to more detailed semi-quantitative measurements over a 256 μm^2 region. Especially channel side of inhomogeneous coating GDL measured the region where the oxygen signal was strong shown in Fig. 14 (Inhomo-a 6000 h). On the other hand, the oxygen content in the homogeneous coated GDLs was corrected to account for the fraction originating from the Cytop, using the fluorine peak intensity and the known composition of Cytop. The results are shown in Table 4. A large increase in the amount of oxygen present on the channel side of the inhomogeneous coating GDL was observed, compared with the homogeneous coating GDL.

3.2.6. Surface adsorbate on the GDL with TOF-SIMS

The EPMA results indicated an increase in the amount of oxygen on the surface of the channel side of the inhomogeneous GDL which showed degradation in the polarization (Section 3.1.1). This surface was also examined with TOF-SIMS to determine the chemical species present.

Comparisons of the relative amounts of surface chemical species for homogeneous coating and inhomogeneous coating GDL are shown in Figs. 15 and 16, respectively. The observed peaks were standardized by the $31CF^+$ peak for positive ion data and the CF_3^- peak for negative ion data. The relative intensities of secondary positive and negative ions are shown in Fig. 15(a), Fig. 16(a) and Fig. 15(b), Fig. 16(b), respectively.

When the homogeneous coating GDL and inhomogeneous coating GDL were compared, stronger $C_xF_yO^-$ and $C_xF_yO^+$ signals were observed from the homogeneous coating GDL, reflecting the molecular constitution of Cytop. Moreover, slightly strong CFO^-, CF_3O^-, $C_2F_5O^-$ and $C_3F_5O^-$ signals were observed from the inhomogeneous coating GDL following 6000 h of operation. It is thought that these originated mainly from the polymer electrolyte, since components such as $C_2F_3SO_4^-$ and $C_4F_8SO_4H^-$ were detected, which are hereafter referred to as decomposed polymer electrolyte compounds (DPECs).

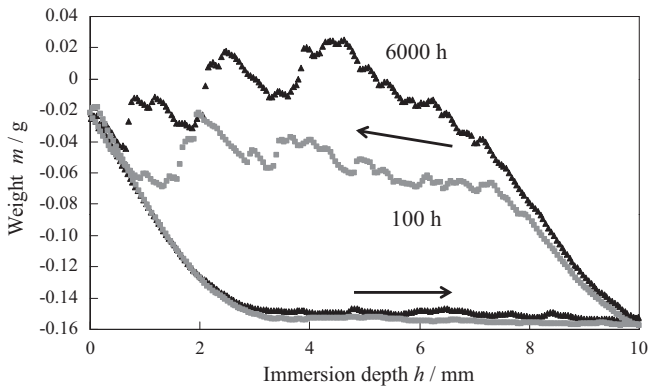

Fig. 13. Hysteresis of immersion cycle of GDL by Wilhelmy method.

Almost no $C_xF_yO^-$ or $C_xF_yO^+$ signals were observed in the unused inhomogeneous coating GDL.

A large amount of DPECs, hydrocarbons and the sulphated compounds were detected in the inhomogeneous coating GDL following 6000 h of operation compared with the unused inhomogeneous coating GDL. However, the adhesions like DPECs and the sulphated compounds increased on GDL operated for 100 h. Moreover, increases in the peak intensities associated with surface oxidation, such as O^-, OH^- and C_2HO^-, were observed for the inhomogeneous coating GDL on cathode operated for 6000 h compared with inhomogeneous coating GDL on cathode operated for 100 h and the unused inhomogeneous coating GDL. Although the increase is detected on the GDL operated for 100 h, it is small compared with the adhesions like DPECs and the sulphated compounds.

Next, a comparison is made between the cathode channel side, the cathode CL side, the anode channel side, and the anode CL side of the homogeneous coating GDL operated for 6000 h, and the homogeneous coating GDL operated for 100 h.

Large amounts of DPECs were detected on these GDLs. They were detected most strongly on the cathode channel side, next on the cathode CL side and then on the other sides. A roughly similar tendency was found for hydrocarbon and sulphated compounds.

Next, the cathode channel sides of GDLs with different waterproofing treatments are compared. The following tendencies were observed for sulphated compounds, Ca^+ and peaks associated with surface oxidation species such as O^-, OH^- and C_2HO^-.

Sulphated compounds were detected at almost the same levels in the homogeneous coating GDLs operated for 100 and 6000 h, and inhomogeneous GDL operated for 100 and 6000 h. Ca^+ was detected most strongly in the homogeneous coating GDL operated for 6000 h, followed by the inhomogeneous coating GDL operated for 6000 h, the homogeneous coating GDL operated for 100 h and finally the inhomogeneous coating GDL operated for 100 h.

O^-, OH^- and C_2HO^- were detected most strongly in the inhomogeneous coating GDL operated for 6000 h, followed by the homogeneous coating GDL operated for 6000 h. The inhomogeneous and the homogeneous coating GDL operated for 100 h were almost the same.

Next, the results of TOF-SIMS mapping for the homogeneous coating GDL in the area as shown in Fig. 4 are presented. A secondary positive ion image of the channel side of the homogeneous coating GDL operated on the cathode for 6000 h is shown in Fig. 17(a). Ca^+ was detected along a straight line through the center of the measured area. This lay on the dividing line between the channel and the rib and corresponded to a white deposit observed with an optical microscope, as shown in Fig. 17(b).

Secondary negative ion images of the channel side of the homogeneous coating GDL operated on the cathode for 100 and 6000 h are shown in Figs. 18 and 19(a), respectively. In both cases, peaks due to DPECs, hydrocarbons, etc., were strongly observed in an area corresponding not to the surface facing the rib but to the surface facing the channel (not shown except DPECs).

Table 4
Increasing oxygen content on GDL detected with EPMA. Comparison of change rate of oxygen detected with EPMA and chemical species which contain oxygen detected with TOF-SIMS.

		Unused	100 h	6000 h
Homogeneous coating GDL	O mapping by EPMA	74%	100%	83%
	TOF-SIMS (O^-, OH^-, C_2HO^-)	29%	100%	168%
	TOF-SIMS (SO^{3-}, SO^{4-}, $C_2F_3SO^{4-}$, $C_4F_8SO_4H^-$, $C_5F_8SO_6H^-$)	12%	100%	251%
Inhomogeneous coating GDL	O mapping by EPMA	18%	100%	788%
	TOF-SIMS (O^-, OH^-, C_2HO^-)	18%	100%	543%
	TOF-SIMS (SO^{3-}, SO^{4-}, $C_2F_3SO^{4-}$, $C_4F_8SO_4H^-$, $C_5F_8SO_6H^-$)	6%	100%	397%

As seen in Fig. 19(a), S^- was observed at the same location that Ca^+ was found (see Fig. 17). This suggests that the white deposit shown in Fig. 17(b) may be compound which contains calcium and sulfur.

Secondary negative ion images of the CL side of the homogeneous coating GDL operated on the cathode for 6000 h are shown in Fig. 19(b). The adhesion distribution is seen to be uniform.

Secondary negative ion images of the channel and CL sides of the homogeneous coating GDL operated on the anode for 6000 h are shown in Fig. 20(a) and (b), respectively. In both figures, signals due to the DPECs, SO^{3-} and $C_2F_3SO^{4-}$ are seen to be weak, and a zebra-stripe pattern due to the channel and separator is absent, especially in Fig. 20(a).

Meanwhile, secondary negative ion images of the channel and CL sides of the inhomogeneous coating GDL operated on the cathode for 100 h are shown in Fig. 21(a) and (b), respectively. In both figures, signals due to the DPECs SO^{3-} and $C_2F_3SO^{4-}$ are seen. The same DPECs SO^{3-} and $C_2F_3SO^{4-}$ were hardly detected on the channel and CL sides of the inhomogeneous coating GDL operated on the anode for 100 h, as shown in Fig. 22.

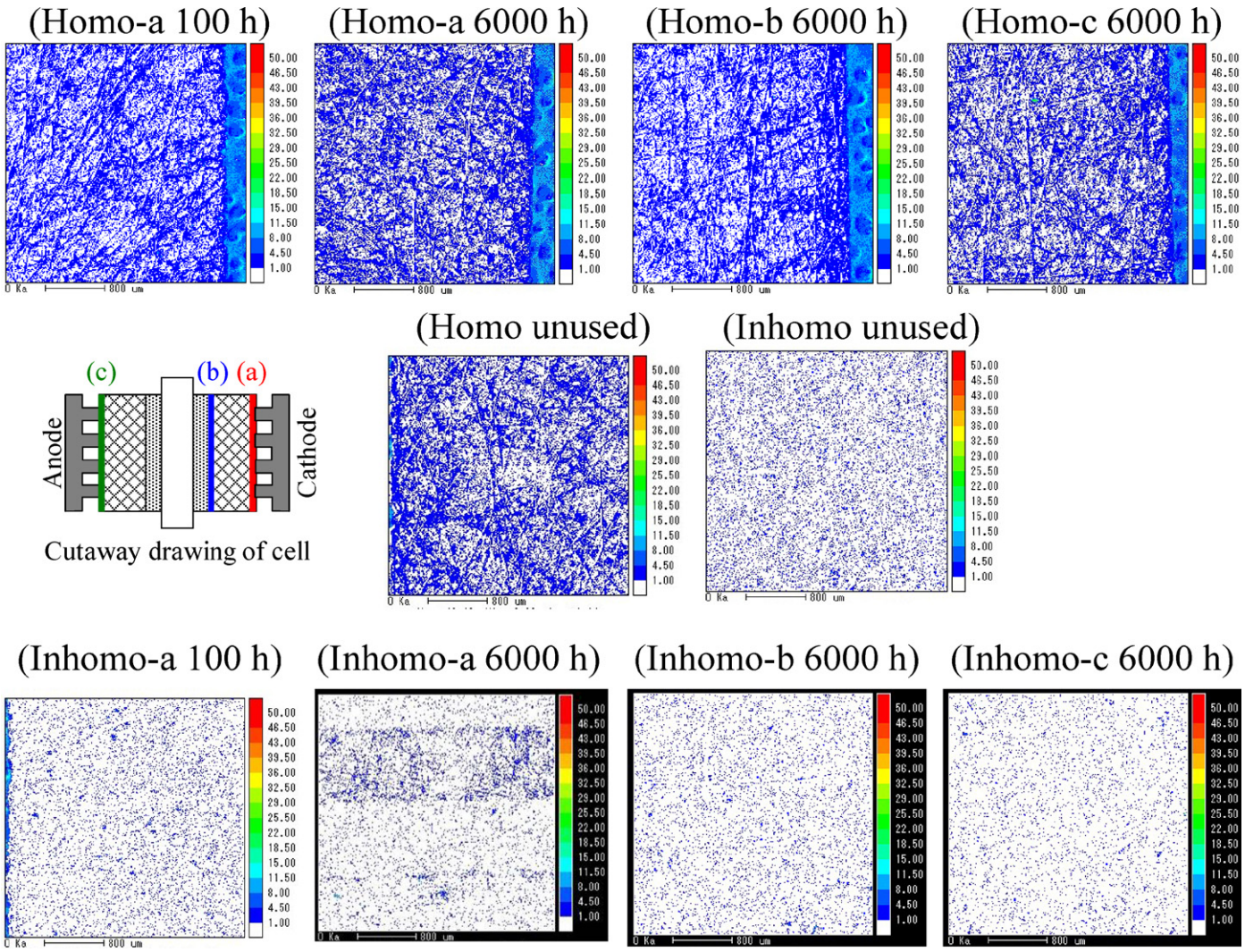

Fig. 14. O mappings of the cathode GDL surface with EPMA. (Homo-a 100 h) and (Homo-a 6000 h) Channel side of homogeneous coating GDL operated on cathode for 100 and 6000 h, respectively. (Homo-b 6000 h) CL side of homogeneous coating GDL operated on cathode for 6000 h. (Homo-c 6000 h) Channel side of homogeneous coating GDL operated on anode for 6000 h. (Homo unused) and (Inhomo unused) Unused homogeneous and inhomogeneous coating GDL, respectively. (Inhomo-a 100 h) and (Inhomo-a 6000 h) Channel side of inhomogeneous coating GDL operated on cathode for 100 and 6000 h, respectively. (Inhomo-b 6000 h) CL side of inhomogeneous coating GDL operated on cathode for 6000 h. (Inhomo-c 6000 h) Channel side of inhomogeneous coating GDL operated on anode for 6000 h.

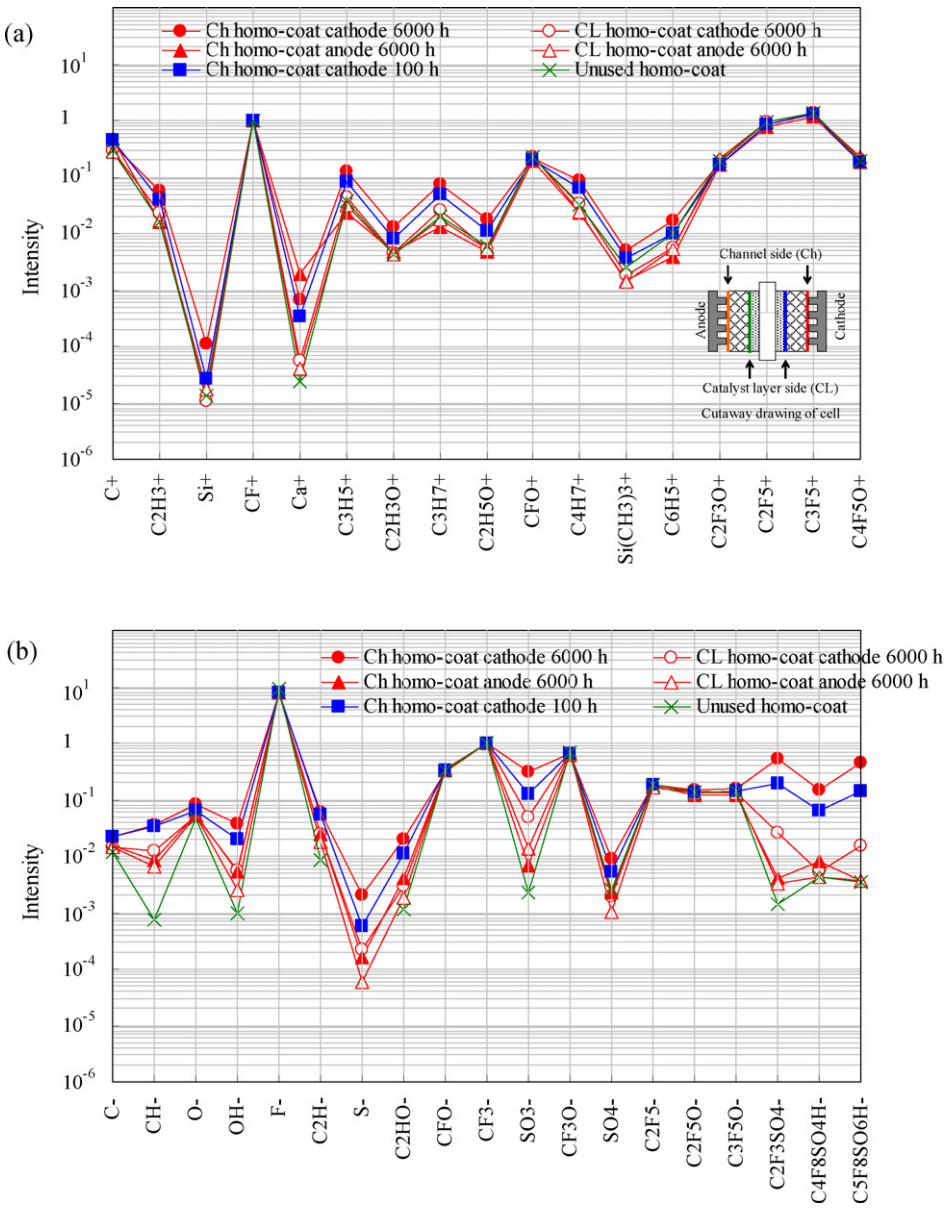

Fig. 15. Comparison of main peaks from homogeneous coating GDL with TOF-SIMS. (a) Secondary positive ion peaks; (b) secondary negative ion peaks.

Lastly, secondary negative ion images of the channel side of the inhomogeneous coating GDL operated on the cathode for 6000 h are shown in Fig. 23. Similar DPECs to those shown in Fig. 19(a) were detected. This and the results of the GDLs operated on the cathode for 100 h suggest that the difference by waterproofing treatments in adsorption might be small. On the other hand, following 6000 h of operation, O^-, which was only weakly detected on the channel side of the homogeneous coating GDL on the cathode, was clearly observed on the channel side of the inhomogeneous coating GDL on cathode.

4. Discussion

In a previous study, carbon corrosion and a decrease in the amount of PTFE on the carbon fibers of the GDL were observed for the degraded GDL under drive cycle conditions [26]. Therefore, it is important to consider both the state of carbon fiber and binder surface and the state of the water-shedding coating. Furthermore, it might be likely that the crystallinity of the carbon fiber and binder greatly also influences the GDL durability since these factors have a large effect on the surface properties and oxidation resistivity like the water-proofing method. The surface roughness of a carbon fiber is also an important factor for wettability degradation.

In this study, two different GDL waterproofing treatments were used. One was treatment with a turbid PTFE dispersion and the other was treatment with a transparent Cytop solution. The PTFE treatment led to uneven coverage as shown in Fig. 1. It might be estimated that the PTFE treatment causes particles of its diameter from 200 to 250 nm to adhere to the carbon fiber. In contrast, the Cytop treatment formed a homogeneous layer since Cytop is a solution.

As seen in Fig. 7, very little change occurred in the overvoltages for the Cytop-treated GDL. On the other hand, the diffusion overvoltage increased for the PTFE-treated GDL. Moreover, it was confirmed that this diffusion overvoltage had its origin in the GDL as shown in Figs. 9 and 10. The degradation control of GDL by the homogeneous coating is clear from the above-mentioned comparison. However, CL degradation also affects the increase in diffusion overvoltage [9]. GDLs of different water management property were used in this study. As shown in Table 2 and Fig. 12, degra-

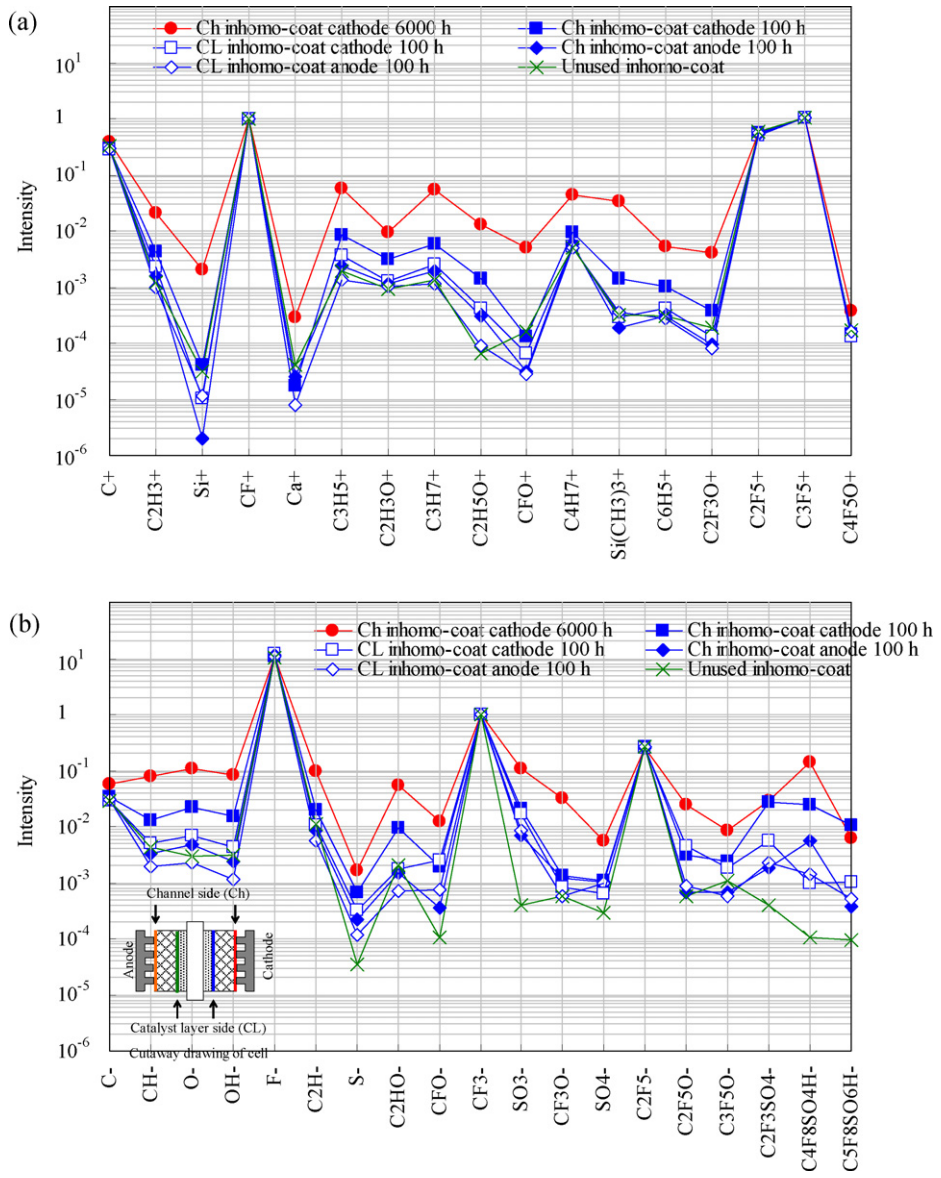

Fig. 16. Comparison of main peaks from inhomogeneous coating GDL with TOF-SIMS. (a) Secondary positive ion peaks; (b) secondary negative ion peaks.

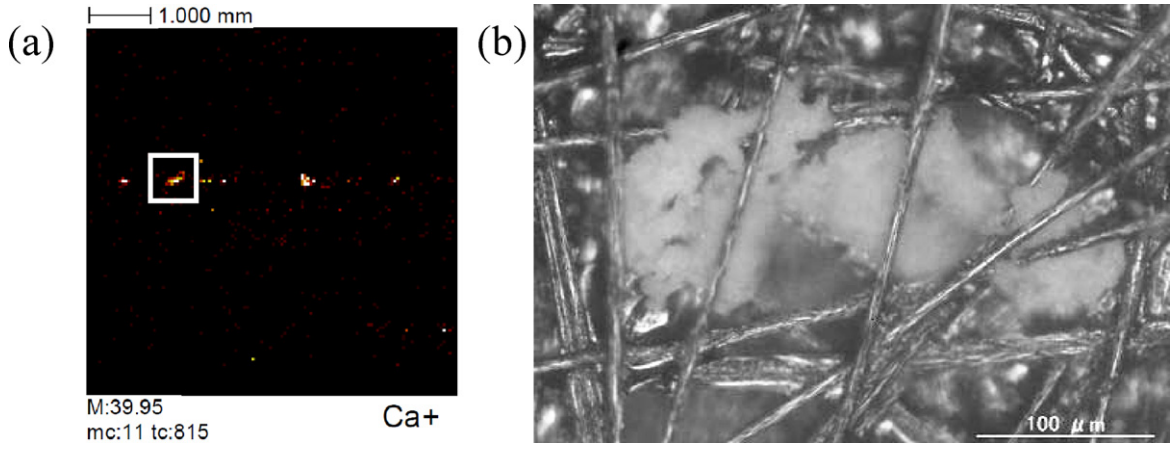

Fig. 17. (a) Secondary Ca^+ ion image of channel side of homogeneous coating GDL operated on cathode for 6000 h with TOF-SIMS. (b) Optical observation of the same area of homogeneous coating GDL observed with TOF-SIMS.

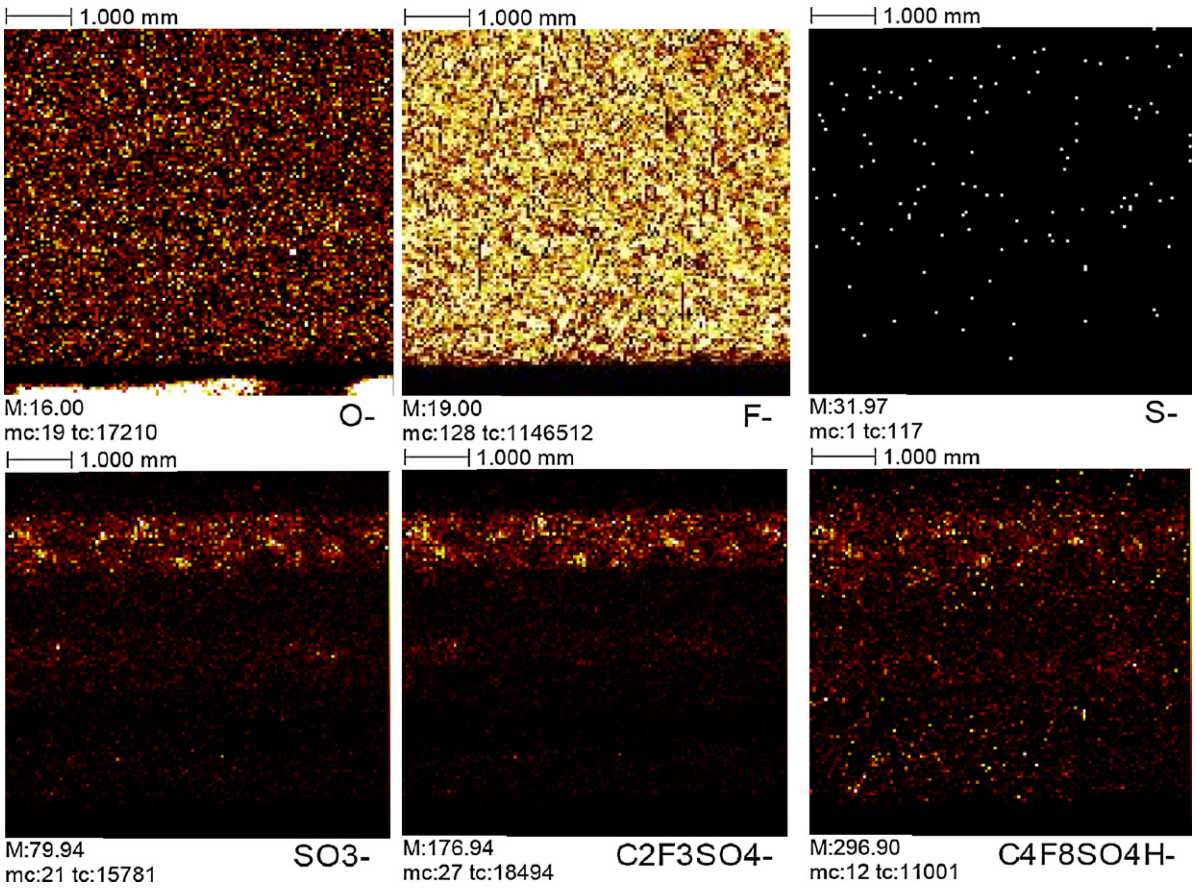

Fig. 18. Secondary negative ion images of channel side of homogeneous coating GDL operated on cathode for 100 h with TOF-SIMS.

dations of CL were seen after 6000 h using each GDL. As shown in Table 2, reduction of the pore volume in CL was large when inhomogeneous coating GDL was used. As shown in Fig. 12, the corrosion of carbon support was large when homogeneous coating GDL was used. These are considered to be a factor of increase of the diffusion overvoltage which does not originate in GDL.

Moreover, when these results are compared with our report argued about humidification condition as experiment parameter [9], in degradation of CL, operation with inhomogeneous coating GDL seems to correspond to high humidification, and operation with homogenous coating GDL seems to correspond to low humidification. Water management performance of GDL may have influenced the humidity in CL. The relation between water management performance of GDL and CL degradation must be verified further.

Analysis of the used GDLs showed that significant changes had occurred, especially on the cathode channel side. As shown in Figs. 15(b), 16(b), 19(a) and 23(a), hydrophilic compounds adhered to the GDL, regardless of water-proofing treatment. Furthermore, even after only 100 h of operation, a non-negligible amount of compounds such as DPECs was found to be adhered to the GDL as shown in Figs. 15(b), 16(b), 19(a) and 21(a).

These results suggest that a large amount of decomposed compounds are released during the early stages of use of the new CCM. However, these adhered compounds did not appear to have any impact on the performance.

Moreover, this grime was found to adhere to the GDL surface facing the cathode separator channels as shown in Figs. 18, 19(a), 21(a) and 23. This suggests that water transport occurs from the inner MEA to the channels of the separator through the cathode electrode. Under these power generation conditions, it is thought that the condensed water was generated under high loading in the polarization measurements. Water-soluble DPECs formed in the MEA then dissolved in this condensed water, and they became dehydrated as they passed through the GDL. It is thought that the water evaporated when the load decreased, and the dissolved material was deposited on the GDL surface.

In this scenario, water buildup should mainly occur not on the area of the GDL facing the rib but rather on the area facing the channel and dissolution should also occur of water-soluble substances from the outside. Little deposition of material should occur on the CL side, since it is kept washed by the condensed water, and evaporation to dryness occurs mainly at the channel side.

In addition, at the anode, the amount of material adhesion at either the channel or CL side is relatively small. Water condensation occurs at the cathode, but it can be assumed that little water condenses at the anode, even taking back diffusion into account.

The use of the homogeneous coating GDL did not have any real effect on the accumulation of such adhered material. Therefore, increasing the adhesion resistance of the GDL by improving its surface properties cannot be expected. However, adhesion of such hydrophilic material may lead to an increase in the wettability of the GDL. Its hydrophobicity can then be said to have decreased, although a receding contact angle of over 90° is still maintained, as shown in Table 3. The origin of the decrease in hydrophobicity cannot be completely clarified, because adhesion of hydrophilic material and some oxidation were simultaneously observed on the homogeneous coating GDL.

However, it is thought that the influence of adhering hydrophilic material is quite small since a large amount of such material is present even after 100 h of operation. In any case, in the present

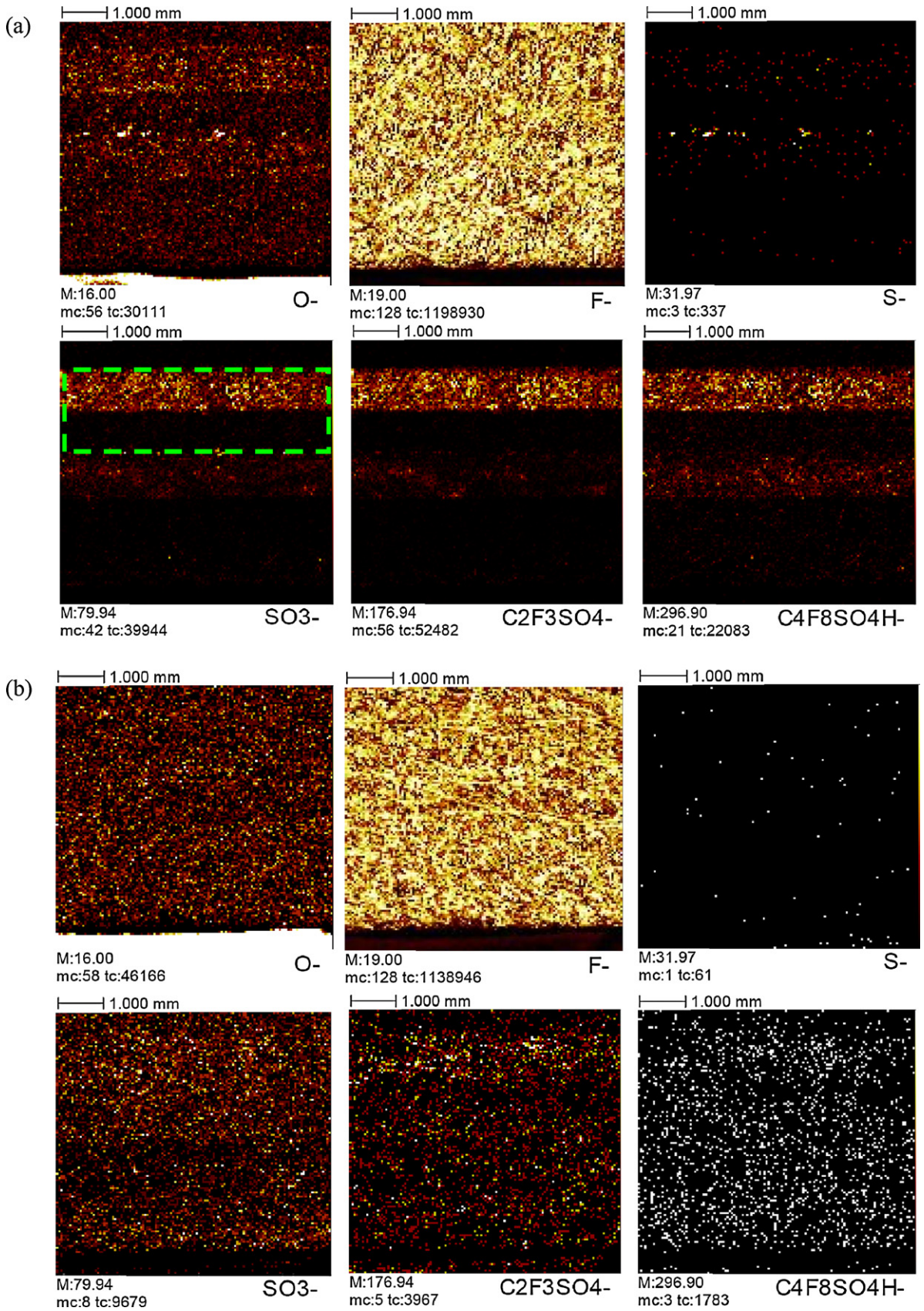

Fig. 19. Secondary negative ion images with TOF-SIMS. (a) Channel side of homogeneous coating GDL operated on cathode for 6000 h. Dashed square area shows the calculation area for Table 4. (b) CL side of homogeneous coating GDL operated on cathode for 6000 h.

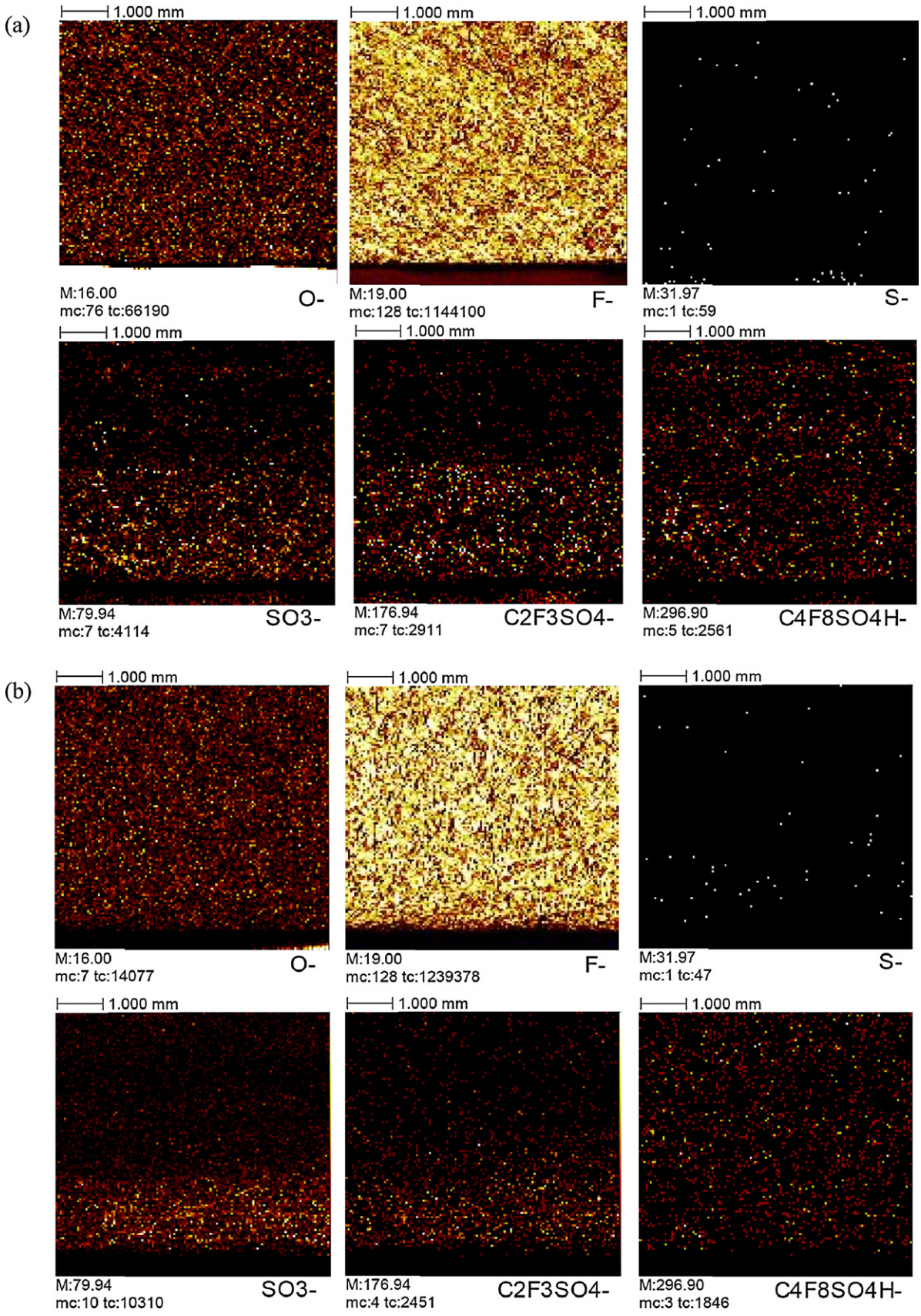

Fig. 20. Secondary negative ion images with TOF-SIMS. (a) Channel side of homogeneous coating GDL operated on anode for 6000 h. (b) CL side of homogeneous coating GDL operated on anode for 6000 h.

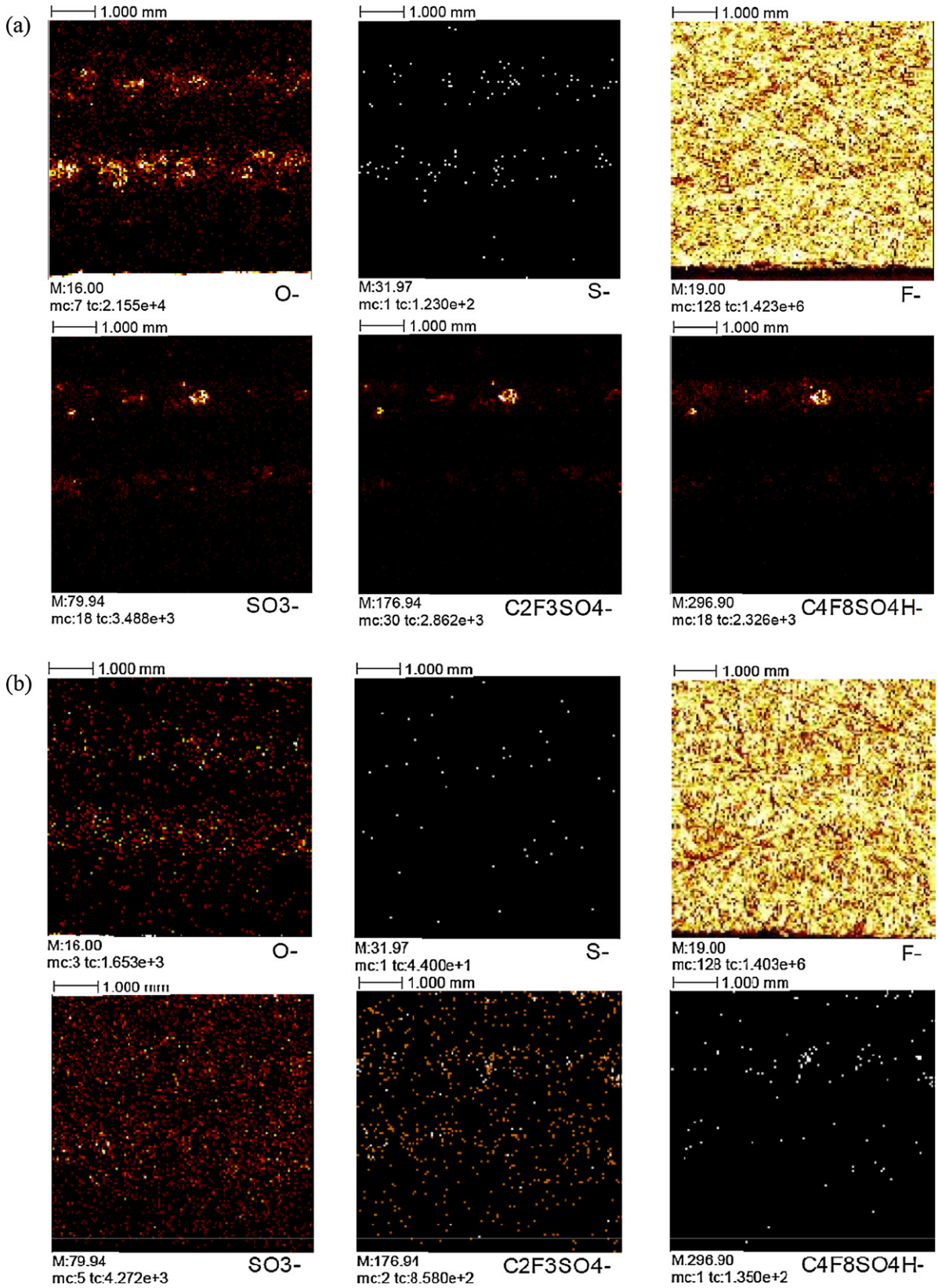

Fig. 21. Secondary negative ion images with TOF-SIMS. (a) Channel side of inhomogeneous coating GDL operated on cathode for 100 h. (b) CL side of inhomogeneous coating GDL operated on cathode for 100 h.

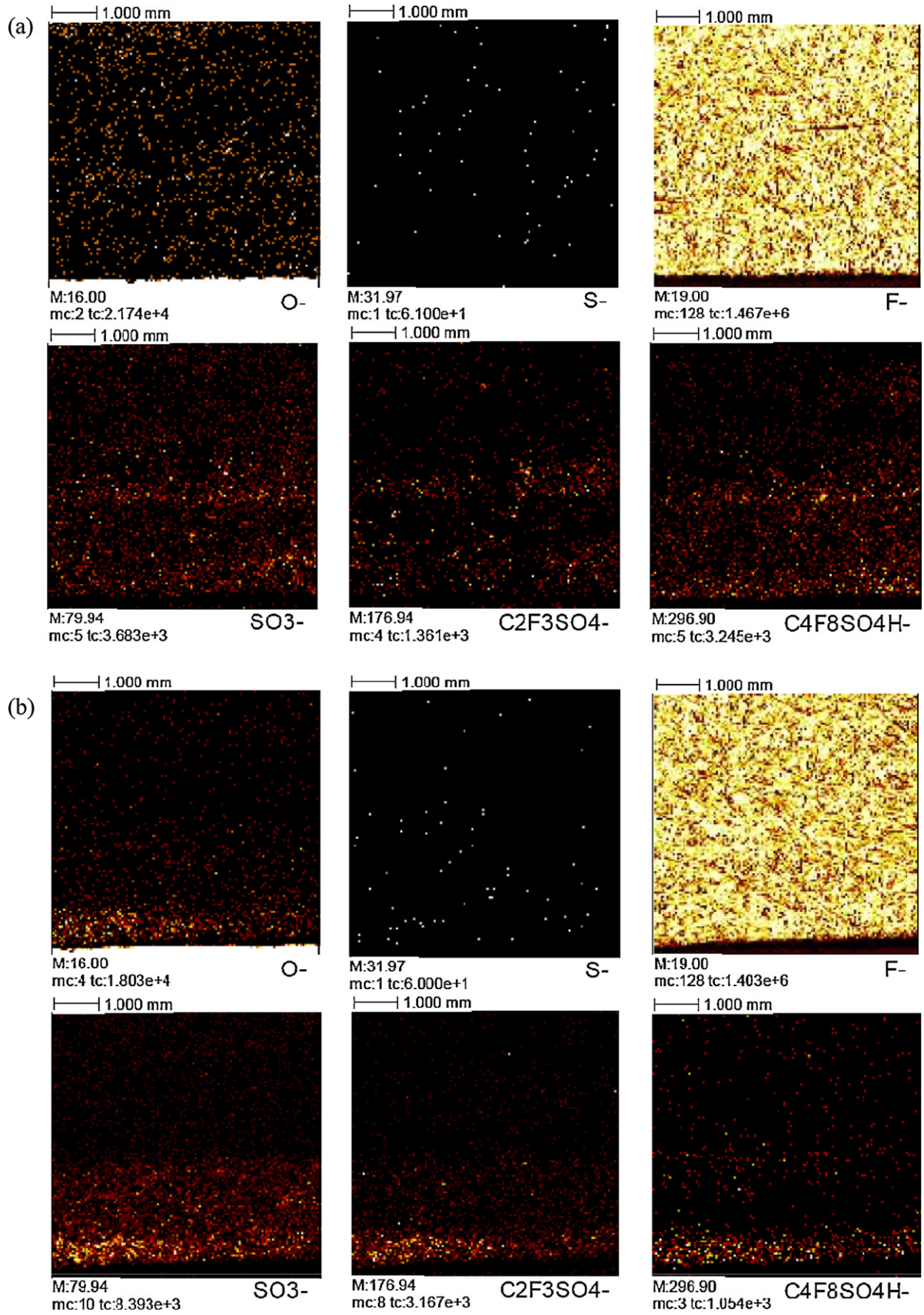

Fig. 22. Secondary negative ion images with TOF-SIMS. (a) Channel side of inhomogeneous coating GDL operated on anode for 100 h. (b) CL side of inhomogeneous coating GDL operated on anode for 100 h.

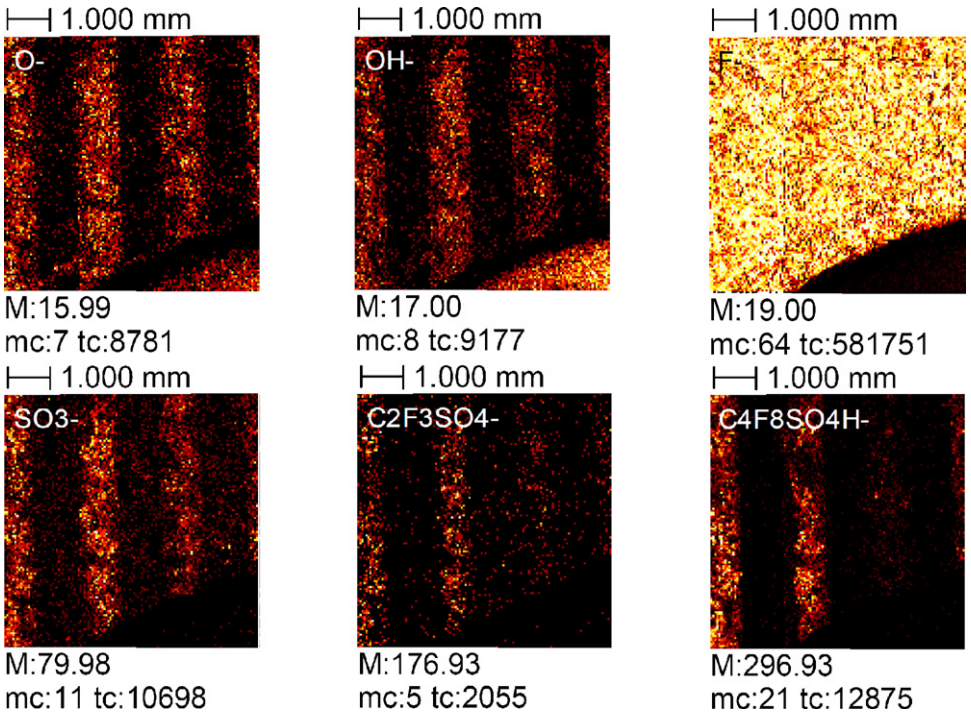

Fig. 23. Secondary negative ion images of channel side of inhomogeneous coating GDL operated on cathode for 6000 h with TOF-SIMS.

study, no correlation was found between the amount of such material and the degree of flooding in the GDL.

It is thought that such hydrophilization of the GDL surface facing the channel influences the mobility of liquid drops in the channel. When it becomes easy for water to adhere there, plugging results, and it becomes a factor in the cell performance. Therefore, it is necessary to consider the possibility of such plugging during long-term operation. In the present study, it is possible that no such degradation was observed because of the use of 16 straight channels that were not easily blocked.

On the other hand, for the inhomogeneous coating GDL, compounds related to oxidation of the carbon surface, such as C_2HO^- OH^-, and O^-, were detected more frequently than for the homogeneous coating GDL (see Figs. 15(b) and 16(b)). The EPMA intensity of oxygen increased remarkably for the inhomogeneous coating GDL on the cathode following 6000 h of operation as shown in Table 4. The TOF-SIMS results are also taken into account in Table 4, it can be assumed that the EPMA signal originates from oxidized regions of the carbon surface. Therefore, it is suggested that oxidation of the carbon fiber surface is the cause of the increase in flooding in the GDL in this case. In addition, this increase in oxygen was also 576% on the CL side of GDL. This indicates the oxidation of carbon fiber occurred on both the channel and the CL side of the GDL. Furthermore, this signal was strongest on the GDL surface facing the separator channels (see Figs. 14 and 23). This suggests a correlation between oxidation of the GDL and water accumulation.

As discussed above, it can be said that the oxidation of the carbon fiber can be controlled by homogeneous coating with the Cytop solution, and the increase in the diffusion overpotential from GDL can be suppressed. Additionally, the application of Cytop to the microporus layer which is often used with a GDL is also likely to be effective in improving its durability. These are interesting topics for a future study.

Although the present study dealt only with the GDL, oxidation of the CL is also an important issue, and it is crucial to investigate which of the two components becomes oxidized more easily, and which has a larger influence on cell degradation. This will be addressed in a future study.

5. Conclusions

In this study, long-term operation of a PEFC with homogeneous coating and inhomogeneous coating GDLs was carried out and the changes in diffusion overvoltage were compared. The results indicated that the increase in the diffusion overvoltage from the GDL could be controlled by the use of a homogeneous coating GDL.

It was shown that the increase in the diffusion overvoltage from the GDL was caused mainly by oxidation of the carbon fiber, and not by the accumulated adhesion of hydrophilic material on the GDL surface.

Acknowledgments

The authors express their thanks to all those who assisted in the writing of this report. This research was performed under a grant from the Water Management Project from the New Energy and Industrial Technology Development Organization (NEDO) for strategic technical development for the practical realization of PEFCs. The GDL contact angle measurements were supported by Mr. Yukihiro Goto and Mr. Hiroyuki Naruke from EKO Instruments Co. Ltd., Japan as part of cooperative research.

References

[1] R. Borup, J. Meyers, B. Pivovar, Y.S. Kim, R. Mukundan, N. Garland, D. Myers, M. Wilson, F. Garzon, D. Wood, P. Zelenay, K. More, K. Stroh, T. Zawodzinski, J. Boncella, J.E. McGrath, M. Inaba, K. Miyatake, M. Hori, K. Ota, Z. Ogumi, S. Miyata, A. Nishikata, Z. Siroma, Y. Uchimoto, K. Yasuda, K. Kimijima, N. Iwashita, Chem. Rev. 107 (2007) 3904–3951.
[2] W. Schmittinger, A. Vahidi, J. Power Sources 180 (2008) 1–14.
[3] Y. Hiramitsu, K. Hirose, K. Kobayashi, M. Hori, Trans. Mater. Res. Soc. Jpn. 33 (2008) 1113–1117.
[4] Y. Hiramitsu, K. Okada, K. Kobayashi, M. Hori, Fiber Preprints 63 (2008) 192.
[5] Y. Hiramitsu, H. Sato, M. Hori, J. Power Sources 195 (2010) 5543–5549.
[6] Y. Hiramitsu, K. Kobayashi, M. Hori, J. Power Sources 195 (2010) 7559–7567.
[7] Y. Hiramitsu, Y. Hayashi, K. Kobayashi, M. Hori, IEEJ Trans. PE 128 (2008) 593–598.
[8] Y. Hiramitsu, Y. Hayashi, K. Kobayashi, M. Hori, Electr. Eng. Jpn. 169 (2009) 10–17.
[9] Y. Hiramitsu, H. Sato, H. Hosomi, Y. Aoki, T. Harada, Y. Sakiyama, Y. Nakagawa, K. Kobayashi, M. Hori, J. Power Sources 195 (2010) 435–444.

[10] R. Borup, J.R. Davey, F.H. Garzon, D.L. Wood, M.A. Inbody, J. Power Sources 163 (2006) 76–81.
[11] J. Wang, G. Yin, Y. Shao, S. Zhang, Z. Wang, Y. Gao, J. Power Sources 171 (2007) 331–339.
[12] Z. Siroma, N. Fujiwara, T. Ioroi, S. Yamazaki, H. Senoh, K. Yasuda, K. Tanimoto, J. Power Sources 172 (2007) 155–162.
[13] S. Maass, F. Finsterwalder, G. Frank, R. Hartmann, C. Merten, J. Power Sources 176 (2008) 444–451.
[14] Y. Aoki, Y. Tanahashi, Y. Nakagawa, Y. Hiramitsu, M. Hori, Proceedings of the 16th FCDIC Fuel Cell Symposium, 2009, pp. 233–236.
[15] M. Nose, T. Kinumoto, H.-S. Choo, Y. Iriyama, T. Abe, Z. Ogumi, Proceedings of the 15th FCDIC Fuel Cell Symposium, 2008, pp. 243–246.
[16] M. Nose, T. Kinumoto, H.-S. Choo, K. Miyazaki, T. Abe, Z. Ogumi, Fuel Cells 9 (2009) 284–290.
[17] M. Nose, T. Kinumoto, H.-S. Choo, K. Miyazaki, T. Abe, Z. Ogumi, Chem. Lett. 38 (2009) 788–789.
[18] H.-S. Choo, T. Kinumoto, M. Nose, K. Miyazaki, T. Abe, Z. Ogumi, J. Power Sources 185 (2008) 740–746.
[19] T. Kinumoto, M. Toyoda, H.-S. Choo, M. Nose, Y. Iriyama, T. Abe, Z. Ogumi, ECS Trans. 13 (2008) 111–118.
[20] T. Ioroi, H. Senoh, S. Yamazaki, Z. Siroma, N. Fujiwara, K. Yasuda, J. Electrochem. Soc. 155 (2008) B321–B326.
[21] A. Masao, S. Noda, F. Takasaki, K. Ito, K. Sasaki, Electrochem. Solid-State Lett. 12 (2009) B119–B122.
[22] F. Takasaki, Z. Noda, A. Masao, Y. Shiratori, K. Ito, K. Sasaki, ECS Trans. 25 (2009) 831–837.
[23] D. Wood, J. Davey, F. Garzon, P. Atanassov, R. Borup, Proc. Fuel Cell Semin. (2005), CD-ROM.
[24] D. Wood, J. Davey, P. Atanassov, R. Borup, Meet. Abstr. Electrochem. Soc. 602 (2006) 641.
[25] D. Wood, J. Davey, F. Garzon, P. Atanassov, R. Borup, Meet. Abstr. Electrochem. Soc. 502 (2006) 1010.
[26] R. Borup, R. Mukundan, J. Davey, D. Wood, T. Springer, Y.S. Kim, J. Spendelow, T. Rockward, B. Pivovar, M. Arif, D. Jacobson, D. Hussey, K. Chen, K. More, P. Wilde, T. Zawodzinski, V. Gurau, W. Johnson, S. Cleghorn, DOE Hydrogen Program 2007 Annual Merit Review Proceedings, 2007.
[27] Y. Hiramitsu, H. Sato, K. Kobayashi, M. Hori, H. Hosomi, Y. Aoki, Y. Sakiyama, Y. Nakagawa, Proceedings of the 15th FCDIC Fuel Cell Symposium, 2008, pp. 90–93.
[28] S. Takeguchi, E. Yasumoto, Proceedings of the 15th FCDIC Fuel Cell Symposium, 2008, pp. 60–63.
[29] G. Chen, H. Zhang, H. Ma, H. Zhong, Int. J. Hydrogen Energy 34 (2009) 8185–8192.
[30] T. Aoki, A. Matsunaga, Y. Ogami, A. Maekawa, S. Mitsushima, K. Ota, H. Nishikawa, J. Power Sources 195 (2010) 2182–2188.